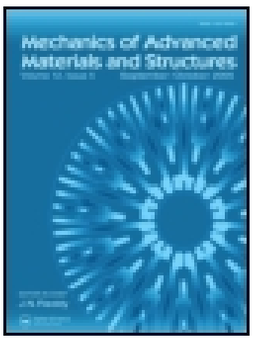

Mechanics of Advanced Materials and Structures

ISSN: 1537-6494 (Print) 1537-6532 (Online) Journal homepage: http://www.tandfonline.com/loi/umcm20

Validation simulation for free vibration and buckling of cracked Mindlin plates using phase-field method

Duc Hong Doan, Thom Van Do, Phuc Minh Pham & Nguyen Dinh Duc

To cite this article: Duc Hong Doan, Thom Van Do, Phuc Minh Pham & Nguyen Dinh Duc (2018): Validation simulation for free vibration and buckling of cracked Mindlin plates using phase-field method, Mechanics of Advanced Materials and Structures, DOI: 10.1080/15376494.2018.1430262

To link to this article: https://doi.org/10.1080/15376494.2018.1430262

Published online: 13 Feb 2018.

MECHANICS OF ADVANCED MATERIALS AND STRUCTURES
2018, VOL. 0, NO. 0, 1–10
https://doi.org/10.1080/15376494.2018.1430262

Taylor & Francis
Taylor & Francis Group

ORIGINAL ARTICLE

Validation simulation for free vibration and buckling of cracked Mindlin plates using phase-field method

Duc Hong Doan[a], Thom Van Do[b], Phuc Minh Pham[c], and Nguyen Dinh Duc[a,d]

[a]Advanced Materials and Structures Laboratory, VNU, Hanoi, University of Engineering and Technology, Cau Giay, Hanoi, Vietnam; [b]Department of Mechanics, Le Quy Don Technical University, Bac Tu Liem, Hanoi, Vietnam; [c]Faculty of Basic Sciences, University of Transport and Communications, Dong Da, Hanoi, Vietnam; [d]Infrastructure Engineering Program, VNU, Hanoi, Vietnam-Japan University, Tu Liem, Hanoi, Vietnam

ABSTRACT

This article focus on validation phase-field method for simulation of free vibration and buckling of crack plates. The formula is derived from using Reissner-Mindlin plate theory. Validation simulation is carried out by numerically investigating free vibration and buckling of cracked plate with taking the configuration, material property, crack location, and other relevant assumptions as the same with the comparing references. The article shows that phase-field approach can be used to estimate the critical buckling load and frequencies of vibration mode. The article also demonstrates the significant advanced of phase-field method for plates with complex crack geometries.

ARTICLE HISTORY
Received 5 September 2017
Accepted 11 January 2018

KEYWORDS
Free vibration; buckling; validation simulation; Reissner-Mindlin plates theory; phase-field method

1. Introduction

Cracks appear in many structures such as plate and shell so that studying the behavior of cracked plates, shells, and other structures is very important. There are some common ways to study the fracture in plate and shell such as finite element method (FEM), extend FEM (XFEM), isogeometric analysis (IGA), phase-field method, …Kim and Glaucio [33] presented mixed-mode crack growth in two-dimensional functionally graded materials based on FEM. Belytschko et al. [6], Gravouli et al. [14], and Moes et al. [21] used XFEM for studying the crack growth. Rabczuk et al. [24] combined meshfree method and XFEM for simulation cohesive fracture. Wells and Sluys [29] relied on XFEM to utilize crack models for dynamic crack propagation. Mostofizadesh et al. [20] analyzed crack propagation in thin shells subjected to blast loading. Wang et al. [30] used this method for studying dynamic fracture of fluid structure. XFEM was used in Dolbow et al. [12] to model and show the mixed-mode fracture of plate based on Mindlin-Reissner theory, the authors analyzed the stress intensity factors in crack plates. Hughes et al. [16] was the first authors to incorporate IGA, and this method was applied successfully in analysis of fracture mechanics.

It can be said that fracture mechanics in stability or instability analysis of the various advanced structures nowadays get a very important role in engineering field and have the great concentrations from researchers and scientists [34]–[36]. Among the investigations of stability of structures, buckling analysis is one of the most important problem needed to consider. Arani et al. [37] applied the nanotechnology as a single-walled carbon nanotubes (SWCNTs) resting in a concrete column beam as the first study they combined together to explore the nonlinear buckling analysis, Kolahchi et al. [38], [39] also used this reinforced nanostructure (SWCNTs) to examine the nonlinear dynamic stability of embedded temperature-dependent viscoelastic plates, and investigate the nonlocal dynamic buckling behavior of embedded microplates reinforced once again with SWCNTs by using Bolotin method. Kolachi [40] was also the first researcher give the study of the dynamic buckling of sandwich nanoplates by using visco-nonlocal-refined zigzag theories, or another study by Bilouei et al. [41] in buckling analysis in concrete column improved with nanofiber reinforced polymer (NFRP). On the other hand, vibration problems also have a big position in considering the stability of the structures. Madani et al. [42] used differential cubature method to research the reinforced complex material as functionally graded cacbon nanotubes embedded in piezoelectric cylindrical shell when applied uniform and nonuniform temperature distribution in the model, Mohammad et al. [43] made the investigation of concrete pipe covered by SiO_2 nanopartical and fiber reinforced plate layer in seismic behavior testing in underwater fluid conveyer as applying the inner and outer fluids like the external forces.

It is clear that there are several method to examine and analyze the behaviors of structures in stability or instabilty problems, especially with the impact of fractures. Recently, phase-field method gets many focus from researchers due to its advantages in fracture mechanic peoblems such as cracking. Borden et al. [7] used the higher isogeometric basis functions and higher-order phase-field model to study the brittle fracture. Schillinger et al. [26] showed isogeometric collocation methods for phase-field fracture models. Bhardwaj et al. [32] explored the numerical simulation of cracked plate using extended IGA under different loads and boundary conditions.

CONTACT Nguyen Dinh Duc ducnd@vnu.edu.vn Advanced Materials and Structures Laboratory, VNU, Hanoi, University of Engineering and Technology, 144 - Xuan Thuy Street - Cau Giay, Hanoi, Vietnam.
Color versions of one or more figures in this article can be found online at www.tandfonline.com/umcm.

Table 1. Comparison of present results with experimental results for critical buckling load of cracked plate in [25].

Sample number	Crack length (c/H)	Crack inclination (α)	Experimental buckling load (N) [25]	Present (N)	% Diff
c_1	0.1	0	1627	1773	8.97
c_2	0.3		1531	1537	0.39
c_3	0.5		1317	1205	8.50
c_4	0.1	30°	1651	1782	7.94
c_5	0.3		1551	1626	4.83
c_6	0.5		1396	1413	1.21
c_7	0.1	60°	1674	1798	7.40
c_8	0.3		1660	1756	5.78
c_9	0.5		1636	1723	5.31

Table 2. Critical buckling load of cracked plate with different thicknesses.

	L/h			
H/l	50	100	150	200
100	4.43461	0.56065	0.166624	0.0703861
200	4.50089	0.570541	0.169751	0.0717487
300	4.52927	0.574772	0.171106	0.0723457
400	4.54515	0.577109	0.171860	0.0726807
500	4.55545	0.578600	0.172338	0.072893
600	4.56287	0.579655	0.172674	0.073042
700	4.56849	0.580443	0.172924	0.0731528
800	4.57287	0.581053	0.173117	0.073238

Table 3. Critical buckling load of plate with different crack length and inclined angle crack, plate with three cracks.

	Inclined angle crack			
c/H	15°	30°	45°	60°
0.1	0.10078	0.10181	0.10336	0.10527
0.2	0.08355	0.08817	0.09526	0.10277
0.3	0.06635	0.07548	0.08912	0.10134
0.4	0.05357	0.06662	0.08576	0.10124

Table 4. Validation of the obtained frequencies with other methods.

ω_i	c/H	Ref. [17] theoretical	Ref. [17] experimental	Ref. [23] FEM	Present
1	0.1416	0.9931	0.9917	0.9891	0.9858
2	0.1416	0.9989	0.9981	0.9985	0.9935
3	0.1416	0.9837	0.9807	0.9826	0.9987

Table 5. Dimensionless frequencies of cracked plate with different thicknesses $(\omega a_0^2/h_0)\sqrt{\rho(1-\nu^2)/E}$, $(a_0 = 10h_0)$.

	L/h			
H/l	50	100	150	200
100	4.8077	2.4143	1.6113	1.2090
200	4.7668	2.3953	1.5991	1.2000
300	4.7548	2.3900	1.5957	1.1976
400	4.7493	2.3875	1.5942	1.1966
500	4.7462	2.3862	1.5934	1.1960
600	4.7443	2.3854	1.5929	1.1957
700	4.7430	2.3848	1.5926	1.1954
800	4.7421	2.3844	1.5923	1.1953

Areias et al. [4] showed a new formulation and procedure to study the stress intensity factors and arbitrary crack growth in plates and shells. In [3], Areias et al. gave the analysis the cracks in thin shells based on Kirchhoff-Love quadrilateral element and Song et al. [27] used phantom node method and shell element of Belytscho-Lin-Tsay to analyze dynamic crack propagation in shells under impulsive loads. Crack growth in shells fuselage structures was simulated in [11], [22].

Bourdin et al. [8], [9] offered the phase-field method to model the fracture in structures, they were based on and improved Griffith's theory presented by Francfort and Marigo [13]. Then, this method was applied widely in both static and dynamic brittle fractures [1], [2], [10], [15], [18], [19], [31]. But the application of this method to model the fracture in plate and shell has not been used widely. By considering shell as a plate combines with a standard membrane, Ulmer et al. [28] applied phase-field model to analyze the fracture in shells. Areias el al. [5] used finite-strain plates and shells and two independent phase-fields to find out the bending fracture behavior. Recently, Duc et al. [31] have used the phase-field method to study dynamic crack propagation in functionally graded epoxy composite with glass fibers.

In this article, we use phase-field method to study buckling and free vibration of cracked plate, the numerical results of this work is compared with experiment results to show the accuracy of this method. And from this basis we show the effects of some parameters on buckling and free vibration of cracked plate.

The rest of the article is organized as follows: Theoretical formulation of Reissner-Mindlin plate theory is presented in Section 2 involving kinetics and governing equations. Formulation of phase-field for free vibration and buckling analysis of cracked Reissner-Mindlin plates is presented in Section 3. In Section 4, firstly, validation or accuracy study of the developed method is analyzed and presented, then some numerical results for buckling analysis of cracked plate with difference crack length and crack geometries are analyzed and presented in Section 4. Some conclusions drawn from the present work are given in Section 5.

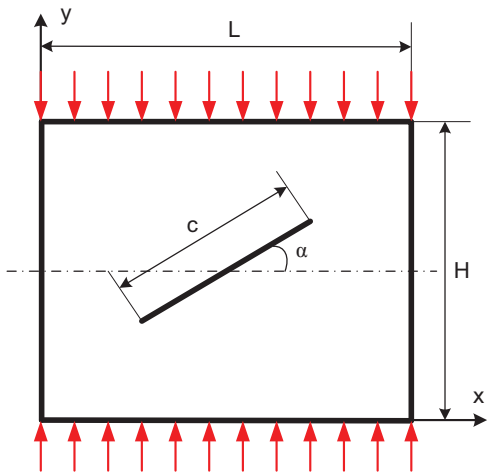

Figure 1. The model geometry of a plate with an inclined central crack.

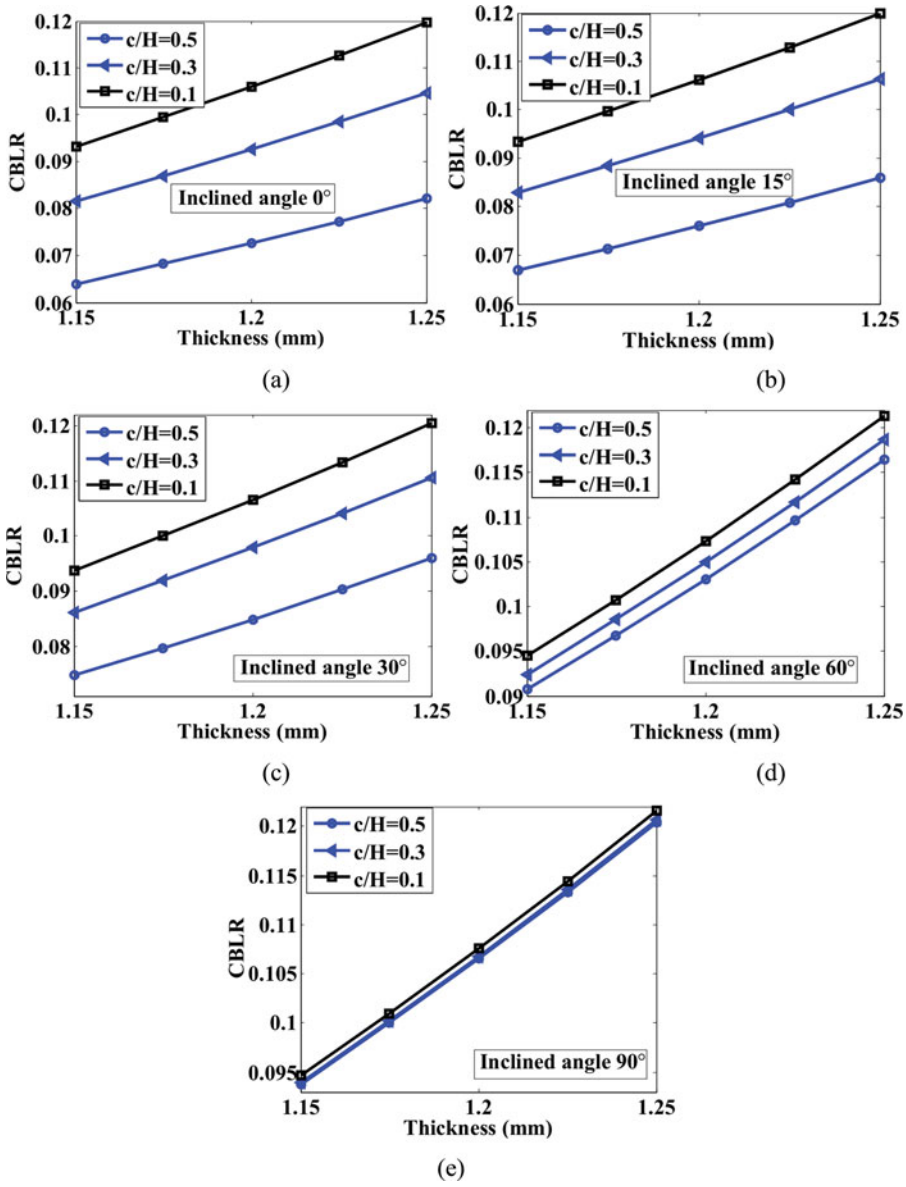

Figure 2. Effect of thickness on CBLR ($L = H = 0.24$ m, CFCF).

2. Formulation for Reissner-Mindlin plate

Using the first-order shear deformation theory of the Reissner-Mindlin formulation, the three-dimensional (3D) displacement field is expressed in term of middle plane as:

$$\begin{aligned} u\left(x,y,z\right) &= u_0\left(x,y\right) + z\beta_x\left(x,y\right) \\ v\left(x,y,z\right) &= v_0\left(x,y\right) + z\beta_y\left(x,y\right) \\ w\left(x,y,z\right) &= w_0\left(x,y\right), \end{aligned} \tag{1}$$

where u, v, w are the displacements components in the x, y, z axes, respectively; β_x, β_y are the transverse normal rotations in the xz and yz planes; and u_0, v_0, w_0 are displacement of middle surface.

From the expression of strains in 3D solid, the strains in terms of mid-plan deformation can be expressed as follow:

$$\boldsymbol{\varepsilon} = \begin{Bmatrix} \boldsymbol{\varepsilon}_p \\ \mathbf{0} \end{Bmatrix} + \begin{Bmatrix} z\boldsymbol{\varepsilon}_b \\ \boldsymbol{\gamma}_s \end{Bmatrix}, \tag{2}$$

where the vector $\boldsymbol{\varepsilon}_p$ and $\boldsymbol{\varepsilon}_b$ contain a membrane, bending and transverse strain, respectively.

$$\boldsymbol{\varepsilon}_p = \begin{Bmatrix} u_{0,x} \\ v_{0,y} \\ u_{0,y} + v_{0,x} \end{Bmatrix}; \quad \boldsymbol{\varepsilon}_b = \begin{Bmatrix} \beta_{x,x} \\ \beta_{y,y} \\ \beta_{x,y} + \beta_{y,x} \end{Bmatrix}; \quad \boldsymbol{\gamma}_s = \begin{Bmatrix} \beta_x + w_{0,x} \\ \beta_y + w_{0,y} \end{Bmatrix}. \tag{3}$$

The potential energy for plate without of cracks can be written as:

$$U\left(\boldsymbol{\delta}\right) = \frac{1}{2}\int_{\Omega}\left\{\boldsymbol{\varepsilon}_p^T\mathbf{A}\boldsymbol{\varepsilon}_p + \boldsymbol{\varepsilon}_p^T\mathbf{B}\boldsymbol{\varepsilon}_b + \boldsymbol{\varepsilon}_b^T\mathbf{B}\boldsymbol{\varepsilon}_p + \boldsymbol{\varepsilon}_b^T\mathbf{D}_b\boldsymbol{\varepsilon}_b + \boldsymbol{\gamma}_s^T\mathbf{D}_s\boldsymbol{\gamma}_s\right\}d\Omega, \tag{4}$$

where $\boldsymbol{\delta}$ is displacement vector, the matrices $\mathbf{A}$, $\mathbf{B}$, $\mathbf{D}_b$, and $\mathbf{D}_b$ are the extensional, bending-extensional coupling, and bending

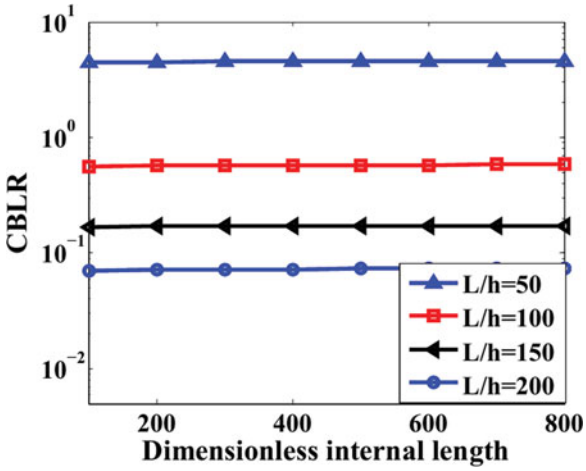

Figure 3. The influence of internal length at different thicknesses ($L = H = 0.24$ m, $c/H = 0.5, \alpha = 0^{\circ}$).

stiffness coefficients and are explicitly given by

$$\mathbf{A} = \frac{Eh}{(1-\nu^2)}\begin{bmatrix} 1 & \nu & 0 \\ \nu & 1 & 0 \\ 0 & 0 & \frac{1}{2}(1-\nu) \end{bmatrix};$$
$$\mathbf{B} = \frac{Eh}{(1-\nu^2)}\begin{bmatrix} 1 & \nu & 0 \\ \nu & 1 & 0 \\ 0 & 0 & \frac{1}{2}(1-\nu) \end{bmatrix} \tag{5a}$$

$$\mathbf{D}_{\mathrm{b}} = \frac{Eh^3}{12\,(1-\nu^2)}\begin{bmatrix} 1 & \nu & 0 \\ \nu & 1 & 0 \\ 0 & 0 & \frac{1}{2}(1-\nu) \end{bmatrix};$$
$$\mathbf{D}_{\mathrm{s}} = \frac{kEh}{2\,(1+\nu)}\begin{bmatrix} 1 & 0 \\ 0 & 1 \end{bmatrix}, \tag{5b}$$

where h is thickness of the plate; E is elastic modulus; and k is transverse shear correction factor.

3. Phase-field model for crack

In phase-field theory of fracture, s is defined a variable phase-field parameter, which continuously varies from 0 to 1. When s equals 0, it means that material phase is fractured, and it is not fractured when s equals 1, if s gets value between 0 and 1 then material in this place is softening. This phase is understood as a progress of microcrack in material and material stiffness is decreased. So that, in phase-field theory, the crack, which is characterized by phase-field fracture variable in range [0,1], forms a narrow band representing the crack in diffusive setting. Because of this formulation, the material contains no explicit discontinuities in materials, and we can have derivation and integral in all domain of analysis. Phase-field variable is taken in strain energy formula of plate by s^2 function, it means that strain energy in cracked area are decreased to 0.

3.1. Vibrational formula for prebuckling analyses

The potential energy for plate subjected to in-plane prebuckling stress can be written as:

$$\begin{aligned} U(\boldsymbol{\delta}, s) = & \left\{ \begin{array}{l} \frac{1}{2}\int_\Omega s^2 \left\{ \boldsymbol{\varepsilon}_p^T \mathbf{A} \boldsymbol{\varepsilon}_p + \boldsymbol{\varepsilon}_p^T \mathbf{B} \boldsymbol{\varepsilon}_b + \boldsymbol{\varepsilon}_b^T \mathbf{B} \boldsymbol{\varepsilon}_p + \boldsymbol{\varepsilon}_b^T \mathbf{D} \boldsymbol{\varepsilon}_b + \boldsymbol{\gamma}_s^T \mathbf{D}_s \boldsymbol{\gamma}_s \right\} d\Omega \\ \quad + \frac{1}{2}\int_\Omega s^2 \left[w_{,x} \; w_{,y} \right] \hat{\sigma}^0 \left[w_{,x} \; w_{,y} \right]^T h d\Omega \\ \quad + \frac{1}{2}\int_\Omega s^2 \left[\phi_{x,x} \; \phi_{x,y} \right] \hat{\sigma}^0 \left[\phi_{x,x} \; \phi_{x,y} \right]^T \frac{h^3}{12} d\Omega \\ \quad + \frac{1}{2}\int_\Omega s^2 \left[\phi_{y,x} \; \phi_{y,y} \right] \hat{\sigma}^0 \left[\phi_{y,x} \; \phi_{y,y} \right]^T \frac{h^3}{12} d\Omega \\ \quad + \int_\Omega G_C h \left[\frac{(1-\nu)^2}{4l} + l|\nabla s|^2 \right] d\Omega \end{array} \right\} \\ = & \left\{ \int_\Omega s^2 \Psi(\boldsymbol{\delta})\, d\Omega + \int_\Omega G_C h \left[\frac{(1-\nu)^2}{4l} + l|\nabla s|^2 \right] d\Omega \right\} \end{aligned} \tag{6}$$

where G_C is the critical energy release rate or surface energy in Griffith's theory and l is a positive regularization constant to regulate the size of the fracture zone.
And

$$\hat{\boldsymbol{\sigma}}^0 = \begin{bmatrix} \sigma_x^0 & \tau_{xy}^0 \\ \tau_{xy}^0 & \sigma_y^0 \end{bmatrix}. \tag{7}$$

The first variation of the functional $U(\boldsymbol{\delta}, s)$ is given by

$$\begin{cases} \delta U(\boldsymbol{\delta}, s, \delta\boldsymbol{\delta}) = 0 \\ \delta U(\boldsymbol{\delta}, s, \delta s) = 0 \end{cases} \tag{8}$$

and then, we have the formulations for prebuckling analyses of cracked plate as

$$\left(\sum \mathbf{K}^e + \lambda_{cr} \sum \mathbf{K}_G^e \right) \boldsymbol{\delta} = 0 \tag{9a}$$

$$\int_\Omega 2s\Psi(\boldsymbol{\delta})\, \delta s d\Omega + \int_\Omega 2G_C h \left[-\frac{(1-\nu)}{4l} + l\nabla s \nabla(\delta s) \right] \times d\Omega = 0 \tag{9b}$$

3.2. Vibrational formula for free vibration

For free vibration analysis of plates, the kinetic energy is expressed as:

$$\mathbf{T}^e = \frac{1}{2}\int_{\Omega_e} s^2 \dot{\mathbf{u}}^T \rho \dot{\mathbf{u}} d\Omega = \frac{1}{2}\dot{\boldsymbol{\delta}}^T \mathbf{M}^e \dot{\boldsymbol{\delta}}. \tag{10}$$

Where the element mass matrix is given by

$$\mathbf{M}^e = \int_{\Omega_e} s^2 \mathbf{L}^T \rho \mathbf{L} d\Omega; \; \mathbf{L} = \begin{bmatrix} 1 & 0 & 0 & z & 0 \\ 0 & 1 & 0 & 0 & z \\ 0 & 0 & 1 & 0 & 0 \end{bmatrix} \tag{11}$$

The Lagrange functional is expressed as

$$\begin{aligned} L(\boldsymbol{\delta}, s) &= T(\boldsymbol{\delta}, s) - U(\boldsymbol{\delta}, s) \\ &= \frac{1}{2}\int_{\Omega_e} s^2 \dot{\mathbf{u}}^T \rho \dot{\mathbf{u}} d\Omega - \frac{1}{2}\int_\Omega s^2 \left\{ \boldsymbol{\varepsilon}_p^T \mathbf{A} \boldsymbol{\varepsilon}_p + \boldsymbol{\varepsilon}_p^T \mathbf{B} \boldsymbol{\varepsilon}_b + \boldsymbol{\varepsilon}_b^T \mathbf{B} \boldsymbol{\varepsilon}_p \right. \\ &\quad \left. + \boldsymbol{\varepsilon}_b^T \mathbf{D} \boldsymbol{\varepsilon}_b + \boldsymbol{\gamma}_s^T \mathbf{D}_s \boldsymbol{\gamma}_s \right\} d\Omega \\ &\quad - \int_\Omega G_C h \left[\frac{(1-\nu)^2}{4l} + l|\nabla s|^2 \right] d\Omega \\ &= \Psi(\boldsymbol{\delta}, s) - \int_\Omega G_C h \left[\frac{(1-\nu)^2}{4l} + l|\nabla s|^2 \right] d\Omega \end{aligned} \tag{12}$$

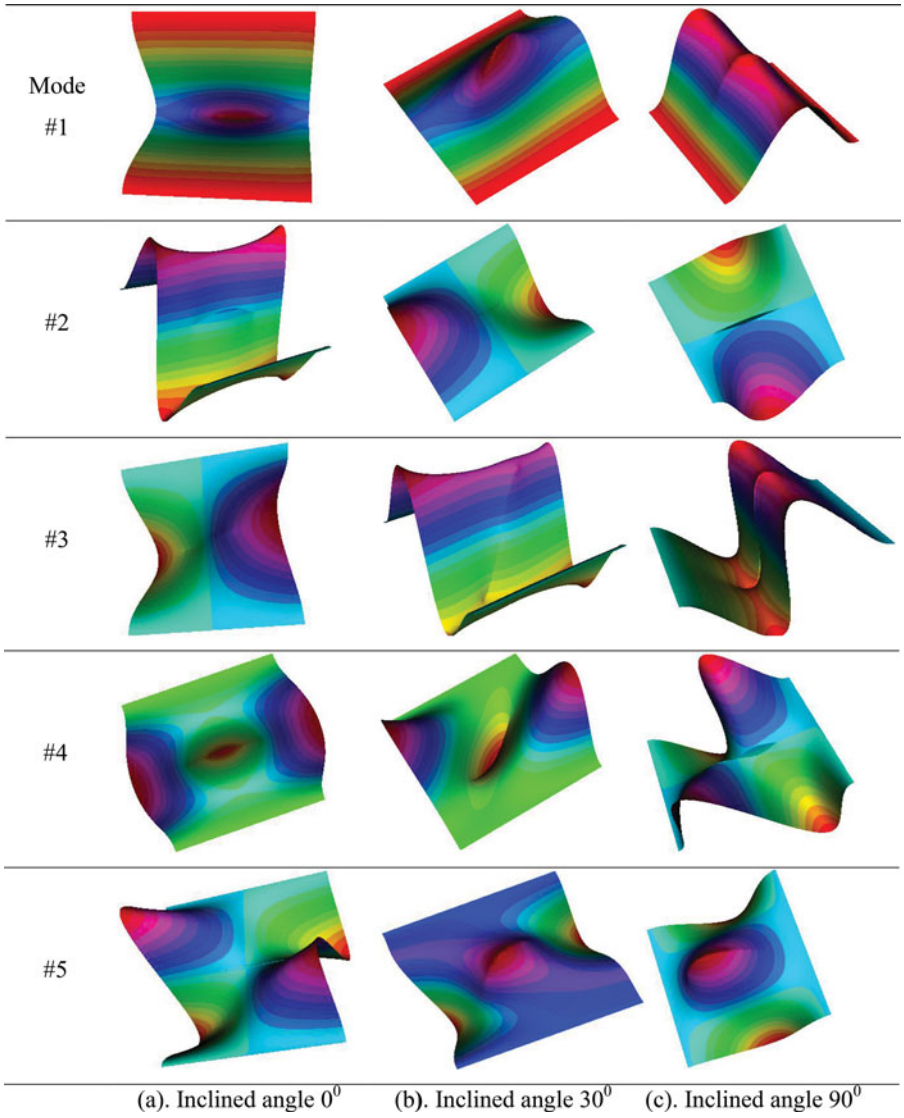

Figure 4 First five buckling modes of CFCF cracked plate ($L = H = 0.24$ m, $h = 1.15$ mm, $c/H = 0.5$, $H/l = 400$).

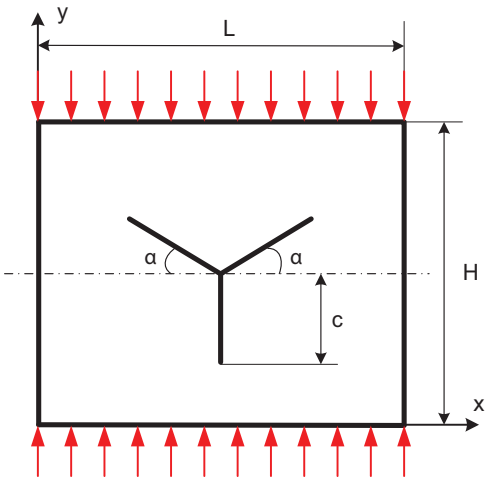

Figure 5. The model geometry of a plate with three cracks and cracks are similar in length.

The first variation of the Lagrange functional is given by

$$\begin{cases} \delta L\left(\boldsymbol{\delta}, s, \delta\boldsymbol{\delta}\right) = 0 \\ \delta L\left(\boldsymbol{\delta}, s, \delta s\right) = 0 \end{cases} \tag{13}$$

Then the eigen values and mode shapes are obtained by solving the following equation:

$$\begin{cases} \left(\sum \mathbf{K}^e + \omega^2 \sum \mathbf{M}^e\right)\boldsymbol{\delta} = 0 & \text{(14a)} \\ \int_\Omega 2s.\Psi\left(\boldsymbol{\delta}\right)\delta s d\Omega + \int_\Omega 2G_C h\left[-\frac{(1-\nu)}{4l} + l\nabla s\nabla\left(\delta s\right)\right] \times d\Omega = 0 & \text{(14b)} \end{cases}$$

4. Numerical results

4.1. *Buckling of cracked plate*

In this section, we study buckling of cracked plates. Firstly, the crack shape is defined by solving Eq. 9b with function $\Psi(\boldsymbol{\delta})$ as following [10]:

$$\Psi\left(\boldsymbol{\delta}\right) = B\frac{G_J}{4l}.H\left(x\right) \tag{15}$$

with

$$H\left(x\right) = \begin{cases} 1 & if\ x \le l_{\text{crack}}\ and\ -\frac{l}{2} \le y \le \frac{l}{2} \\ 0 & else \end{cases} \tag{16}$$

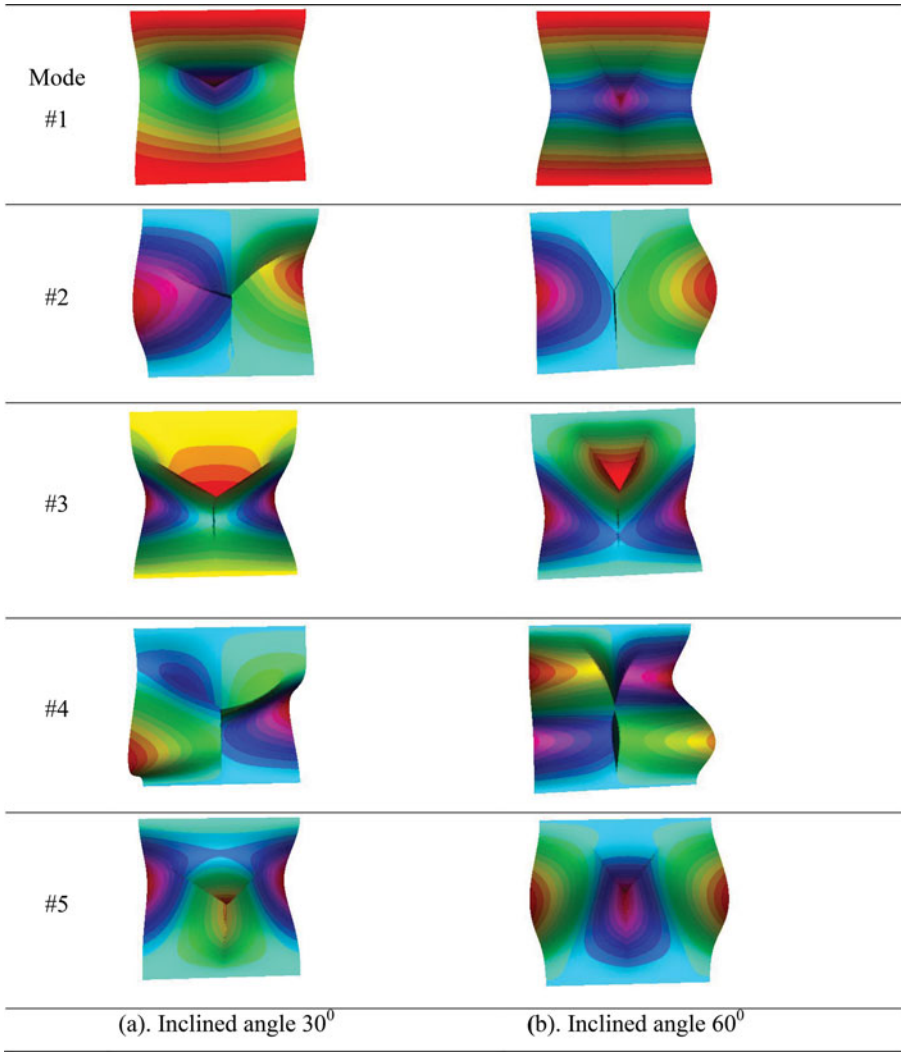

Figure 6. First five buckling modes of CFCF plate with three cracks ($L = H = 0.24$ m, $h = 1.2$ mm, $c/H = 0.5$, $H/l = 400$).

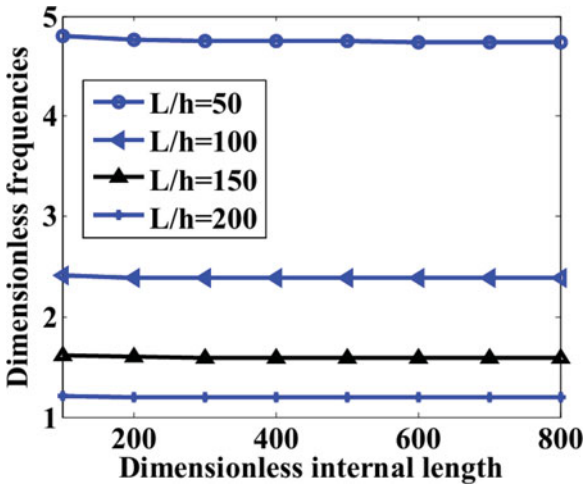

Figure 7. Convergence of internal length at different thicknesses ($L = H = 0.24$ m, $c/H = 0.5$, $\alpha = 0^\circ$, CFCF).

and the scalar B's magnitude can be 10^3, whereas l_{crack} is the length of the crack.

After solving Eq. 9b, we can find out s, and take this value of s to Eq. 9ato get buckling loads and buckling mode shapes.

Firstly, we compare the results of buckling load of cracked plate by this method with experimental results of Seifi et al. [25] as in Table 1, plate with $240 \times 240 \times 12$ mm^3 size, Young modulus $E = 70$ MPa, Poisson ratio 0.33, this plate is compressed in two opposite clamped edges, in the other two edges, the forces are not applied, which can be seen in Figure 1. From Table 1, we can see that the numerical result based on this method is dependable. The maximum error between this numerical results and experimental results reach 9%, this problem is easy to understand because of the error when material producing is not pure and crack size is not perfect. To verify this, we study the effect of plate thickness on critical buckling load of cracked plate.

The plate with $L = H = 0.24$ m is compressed at two opposite edges as Figure 1, thickness h, crack length c, crack inclination α, Young modulus $E = 70$ MPa, and Poisson ratio 0.33. For greater convenience, we define the buckling critical load ratio (BCLR) as follow.

$$BCLR = \frac{100\,(\lambda_{cr})\,a_0}{Eh_0^3}\ (with\ \mathrm{a}_0 = 10h_0) \tag{17}$$

Plate thickness is changed from 1.15 to 1.25 mm, crack angle is changed from 0° to 90°, as we reported in Table 2.

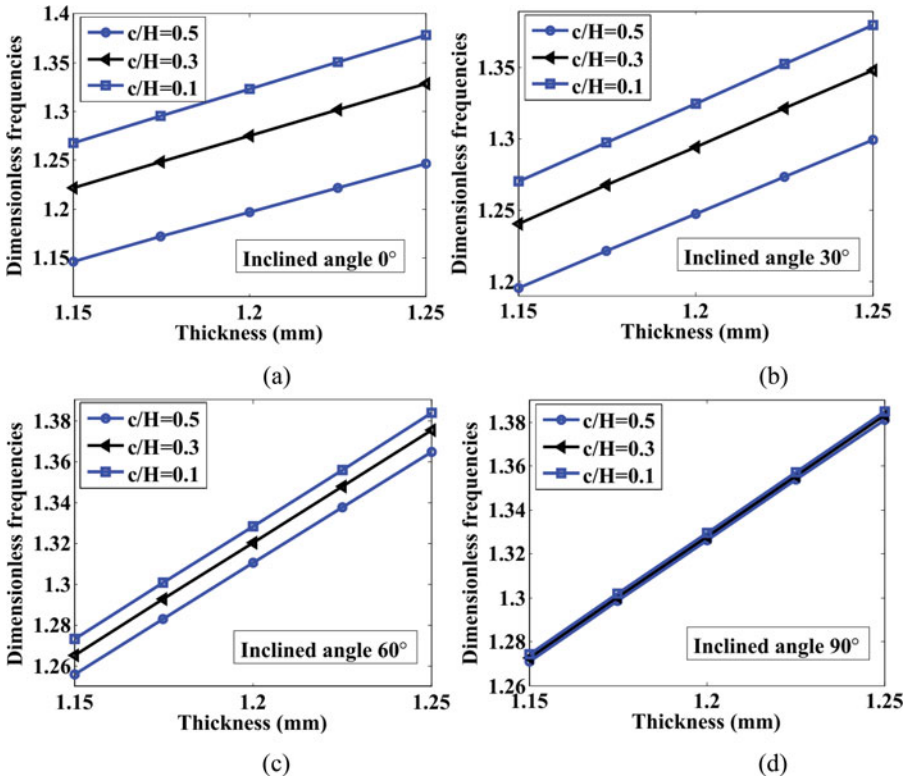

Figure 8. Effect of thickness on frequencies ($L = H = 0.24$ m, CFCF).

We can see that when crack length is increased or plate thickness is decreased, the critical buckling load is decreased as the plate stiffness is decreased. When crack inclination is increased, because the plate is compressed at two opposite edges as in Figure 1, energy release surface at crack is decreased, and this reason makes plate stiffness increased, so that the plate stability is higher. These phenomena agree with results from experiments reported in Seifi et al. [25].

Specially from Figure 2, we can see that with cracked plate as Seifi et al. [25], when plate thickness change about 50 μm from thickness value in Seifi experiment, the critical buckling load will have error from 11.96% to 13.02%. The errors in the results of this work in comparison with Seifi experiment results as in Table 1 are easy to understand.

In the next study, we show the effect of plate thickness on plate stability and examine how the convergence of the method depends on internal length at different thicknesses, we change thickness value with $L/h = 50$–200 and internal length l has value $H/l = 100$–800, we report as in Table 2 and plot as in Figure 3.

From Figure 3, we can see that when H/l gets value from 100 to 800 then the change of critical buckling load is small. On the other hand, internal length l has small effect on results, so that, in all study below we chose internal length value $H/l = 400$.

First five buckling mode shapes of cracked plate at three cases of inclined angle (0°, 30°, and 90°) are plotted in Figure 4. From this we can see that inclined angle of crack has much effect on the shape of cracked plate buckling mode shapes.

Next, to show advantages of this method over the other method, e.g., XFEM method, we study buckling of CFCF square plate with three cracks compressed in two opposite edges as in Figure 5. Plate length L and width H are the same $L = H = 0.24$ m, thickness $h = 1.2$ mm, Young modulus $E = 70$ MPa, and Poisson ratio 0.33, $H/l = 400$, three cracks have the same length c and have cross point at plate center, we change crack length c ($c/H = 0.1$–0.4) and crack angle α from 15° to 60° and report the coefficient buckling as in Table 3.

Table 3 shows that when crack length decreases and rack angle α increases then energy release surface decreases, so that the critical buckling load decreases.

In this case of plate with three cracks have cross point verified that phase-field method can deal with various complexity of crack shape, in which some other method (e.g., XFEM method) cannot solve effectively. Figure 6 plots first five mode buckling shapes in two cases of crack angle (30° and 60°), and it shows that crack angle has effected much on buckling mode shapes of cracked plate.

4.2. *Free vibration of cracked plate*

In this section, we keep studying free vibration of cracked plate. As buckling problem, the crack shape is defined by solving Eq. 14bwith function $\Psi(\boldsymbol{\delta})$ as followed:

$$\Psi(\boldsymbol{\delta}) = B\frac{G_J}{4l}.H(x), \tag{18}$$

where

$$H(x) = \begin{cases} 1 \; if \; x \le l_{crack} \;\; and \;\; \frac{-l}{2} \le y \le \frac{l}{2} \\ 0 \qquad\qquad\quad else \end{cases} \tag{19}$$

with $B = 10^3$.

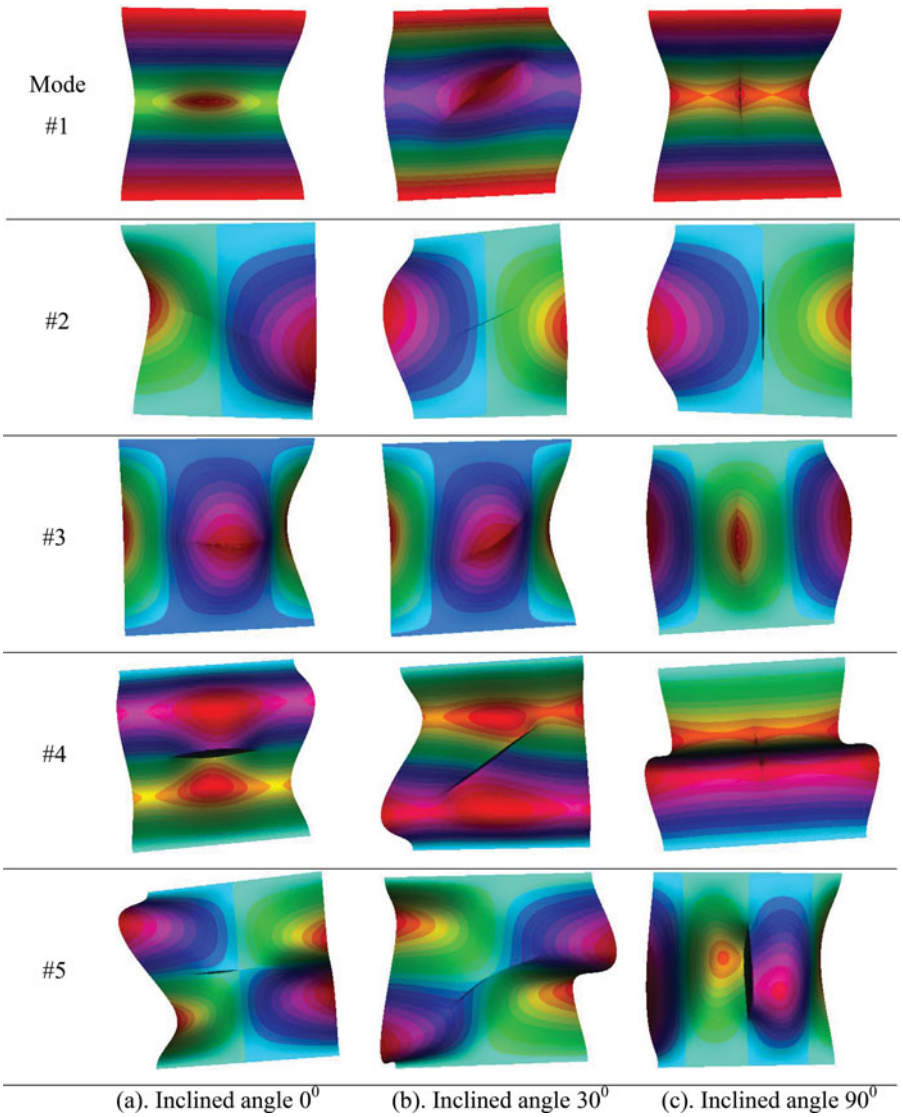

Figure 9. First five mode shapes of CFCF cracked plate ($L = H = 0.24$ m, $h = 1.15$ mm, $c/H = 0.5$, $H/l = 400$).

After solving Eq. 14b, we can get s, and take this value of s to Eq. 14ato find out eigen frequencies and free vibration mode shapes, respectively.

To show the accuracy of this method, frequencies of pure metal cantilever plate with one crack get from the numerical result compared with that experimental, theoretical, and FEM results of other authors, plate with $24 \times 24 \times 2.75$ cm^3 size, Young's modulus $E = 67$ MPa, Poisson's ratio 0.33, and mass density 2800 kg/m^3. The center of the crack is located at the coordinates $x = 9$ cm and $y = 9$ cm. The comparison repotted as in Table 4 shows a small error and this proves the accuracy of this results, note that we chose $l = L/200$.

Based on the method, we use this program to study effect of some parameters on cracked plate frequencies modelled as in Figure 1.

Firstly, we study the effect of plate thickness and internal length, plate with $L = 0.24$ m length, $H = 0.24$ wide and thickness h, internal length $c/H = 0.5$, inclined angle $\alpha = 0^\circ$, Young's modulus $E = 6.7e10$ Pa, Poisson's ratio 0.33, and mass density 2800 kg/m^3, two opposite edges clamped and two edges are free (CFCF), plate thickness changed from $L/h = 50$ to 200, we report the normal frequencies $(\omega a_0^2/h_0)\sqrt{\rho(1-\nu^2)/E}$, with $a_0 = 10h_0$ as in Table 5 and plot these results in Figure 7. We can see that if plate thickness increases, then plate is getting stiffer and frequencies increase, the effect of the internal length changes on frequencies is not significant, so that, from now we choose $H/l = 400$.

Next, we study the effect of crack length, inclined angle, and plate thickness on frequencies of plate with size and properties material as above, but only thickness get value from 1.15–1.25 mm, we plot as in Figure 8. From this figure, we can see that increasing plate thickness or decreasing crack length will make plate getting stiffer and the first frequency will increase, when crack inclined angle increase, with boundary condition CFCF as Figure 1, because energy release surface at crack is decreasing, plate stiff is increasing, so that the frequencies increase.

First five mode shapes of cracked plate with two boundary conditions (CFCF and SSSS) and three inclined angles (0°, 30°, and 90°) are plotted in Figures 9 and 10. These figures show that the boundary condition and crack inclined angle have a significant effect on mode shapes of cracked plate.

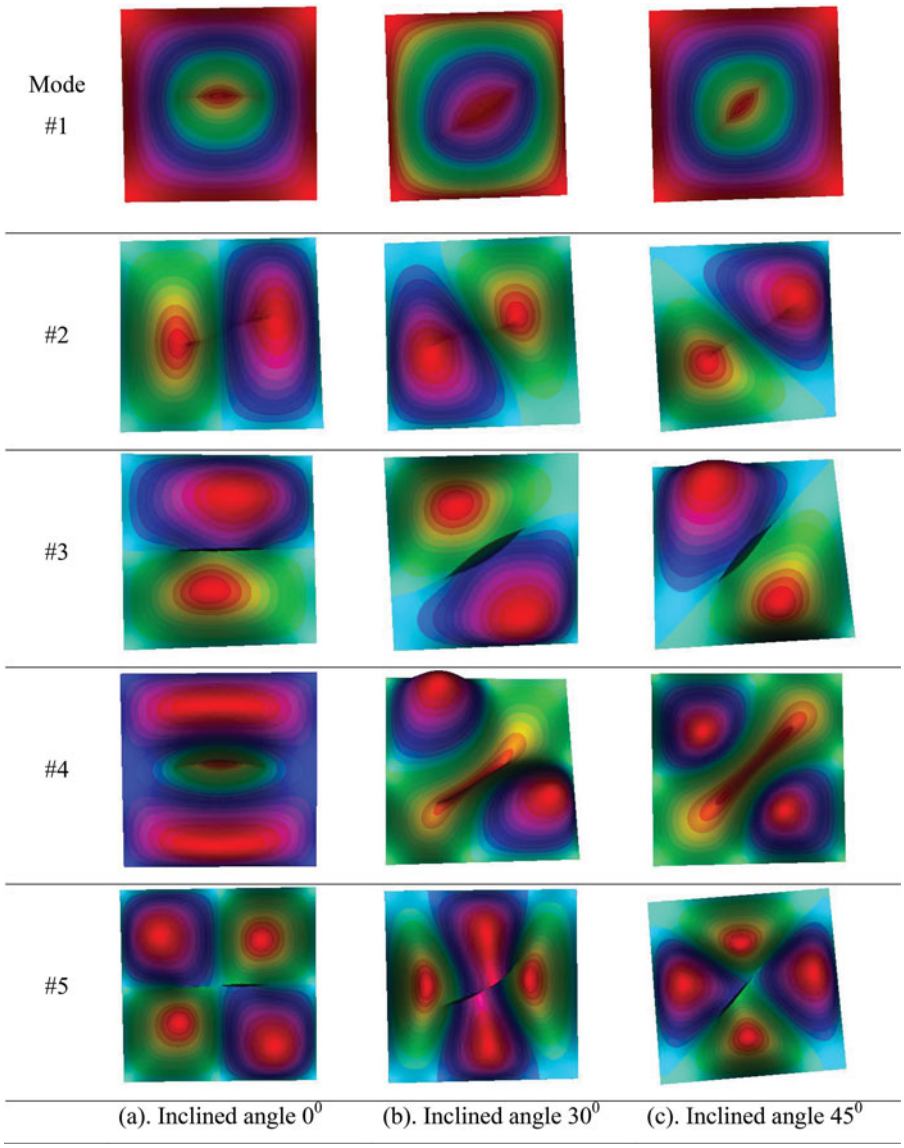

Figure 10. First five mode shapes of SSSS cracked plate ($L = H = 0.24$ m, $h = 1.15$ mm, $c/H = 0.5$, $H/l = 400$).

5. Conclusions

By using phase-filed and based on Reissner-Mindlin plate theory, the article has studied free vibration and static buckling of cracked plate. In cracked plate buckling problem, plate is compressed in two clamped oposite edges while two other edges are free, when the inclined angle and the plate thickness decrease and the crack length increases then the cracked plate is prone for buckling, otherwise the phase-filed method the article used is more advantageous than other method (example XFEM, …) when dealing with plate have complex crack shapes. In problem of free vibration of cracked plate, the article shows that when the plate thickness increases, the crack length decreases and the inclined crack angle increases then the frequencies of cracked plate increase. The obtained results in this article are validated by comparing with other results reported in the open literature.

Funding

This work has been supported by Vietnam National University, Hanoi (VNU, Hanoi), under Project No. QG.17.45.

References

[1] M. Ambati, T. Gerasimov, and L. D. Lorenzis, "A review on phase-field models of brittle fracture and a new fast hybrid formulation", *Comp. Mech.*, vol. 55, pp. 383–405, 2014. doi:10.1007/s00466-014-1109-y.

[2] H. Amor, J. J. Marigo, and C. Maurini, "Regularized formulation of the variational brittle fracture with unilateral contact: Numerical experiments", *J. Mech. Phys. Sol.*, vol. 57, pp. 1209–1229, 2009. doi:10.1016/j.jmps.2009.04.011.

[3] P. M. A. Areias, J. H. Song, and T. Belytschko, "Analysis of fracture in thin shells by overlapping paired elements", *Comp. Meth. Appl. Mech. Eng.*, vol. 195, pp. 5343–5360, 2006. doi:10.1016/j.cma.2005.10.024.

[4] P. M. A. Areias and T. Belytschko, "Non-linear analysis of shells with arbitrary evolving cracks using XFEM", *Int. J. Num. Meth. Eng.*, vol. 62, pp. 384–415, 2005. doi:10.1002/nme.1192.

[5] P. M. A. Areias, T. Rabczuk, and M. A. Msekh, "Phase-field analysis of finite-strain plates and shells including element subdivision", *Comp. Meth. Appl. Mech. Eng.*, vol. 312, pp. 322–350, 2016. doi:10.1016/j.cma.2016.01.020.

[6] T. Belytschko, N. Moes, S. Usui, and C. Parimi, "Arbitrary discontinuities in finite elements", *Int .J. Numer. Meth. Eng.*, vol. 50, pp. 993–1013, 2001. doi:10.1002/1097-0207(20010210)50:4%3c993::AID-NME164%3e3.0.CO;2-M.

[7] M. J. Borden, T. J. R. Hughes, C. M. Landis, and C. V. Verhoosel, "A higher-order phase-field model for brittle fracture: Formulation and analysis within the isogeometric analysis framework", *Comp. Meth. Appl. Mech. Eng.*, vol. 273, pp. 100–118, 2014. doi:10.1016/j.cma.2014.01.016.

[8] B. Bourdin, G. A. Francfort, and J. J. Marigo, "Numerical experiments in revisited brittle fracture", *J. Mech. Phys. Sol.*, vol. 48, pp. 797–826, 2000. doi:10.1016/S0022-5096(99)00028-9.

[9] B. Bourdin, G. A. Francfort, and J. J. Marigo, "The variational approach to fracture", *J. Elast.*, vol. 91, pp. 5–148, 2009.

[10] M. J. Borden, C. V. Verhoosel, M. A. Scott, T. J. R. Hughes, and C. M. Landis, "A phase-field description of dynamic brittle fracture", *Comp. Meth. Appl. Mech. Eng.*, vol. 217–220, pp. 77–95, 2012. doi:10.1016/j.cma.2012.01.008.

[11] C. S. Chen, P. A. Wawrzynek, and A. R. Ingraffea, "Crack growth simulation and residual strength prediction in airplane fuselage", *Technical Report CR-1999-209115*, NASA, Hampton, VA, 1999.

[12] J. Dolbow, N. Moës, and T. Belytschko, "Modeling fracture in Mindlin-Reissner plates with the extended finite element method", *Int. J. Sol. Struct.*, vol. 37, pp. 7161–7183, 2000. doi:10.1016/S0020-7683(00)00194-3.

[13] G. A. Francfort and J. J. Marigo, "Revisiting brittle fractures as an energy minimization problem", *J. Mech. Phys. Sol.*, vol. 46, pp. 1319–1342, 1998. doi:10.1016/S0022-5096(98)00034-9.

[14] A. Gravouil, N. Moes, and T. Belytschko, "Non-planar crack growth by the extended finite element and level sets-part II: Level set update", *Inter. J. Numer. Meth. Eng.*, vol. 53, pp. 2569–2586, 2002. doi:10.1002/nme.430.

[15] T. Gerasimov and L. D. Lorenzis, "A line search assisted monolithic approach for phase-field computing of brittle fracture", *Comp. Meth. Appl. Mech. Eng.*, vol. 312, pp. 276–303, 2016. doi:10.1016/j.cma.2015.12.017.

[16] T. J. R. Hughes, J. A. Cottrell, and Y. Bazilevs, "Isogeometric analysis: CAD, finite elements, NURBS, exact geometry, and mesh refinement", *Comp. Meth. Appl. Mech. Eng.*, vol. 194, pp. 4135–4195, 2005. doi:10.1016/j.cma.2004.10.008.

[17] M. Krawczuk, "Natural vibrations of rectangular plates with a through crack", *Arch. Appl. Mech.*, vol. 63, pp. 491–504, 1993.

[18] C. Kuhn and R. Muller, "A continuum phase field model for fracture", *Eng. Fract. Mech.*, vol. 77, pp. 3625–3634, 2010. doi:10.1016/j.engfracmech.2010.08.009.

[19] C. Miehe, M. Hofacker, and F. Welschinger, "A phase field model for rate-independent crack propagation: Robust algorithmic implementation based on operator splits", *Comp. Meth. Appl. Mech. Eng.*, vol. 199, pp. 2765–2778, 2010. doi:10.1016/j.cma.2010.04.011.

[20] S. Mostofizadeh, M. Fagerström, and R. Larsson, "Dynamic crack propagation in elastoplastic thin-walled structures: Modelling and validation", *Int. J. Num. Meth. Eng.*, vol. 96, pp. 63–86, 2013. doi:10.1002/nme.4524.

[21] N. Moes and T. Belytschko, "Extended finite element method for cohesive crack growth", *Eng. Frac. Mech.*, vol. 69, pp. 813–833, 2002. doi:10.1016/S0013-7944(01)00128-X.

[22] D. O. Potyondy, P. A. Wawrzynek, and A. R. Ingraffea, "Discrete crack growth analysis methodology for through cracks in pressurized fuselage structures", *Int. J. Num. Meth. Eng.*, vol. 38, pp. 1611–1633, 1995. doi:10.1002/nme.1620381003.

[23] G. L. Qian, S. N. Gu, and J. S. Jiang, "A finite element model of cracked plates application to vibration problems", *Compos. Struct.*, vol. 39, pp. 483–487, 1991. doi:10.1016/0045-7949(91)90056-R.

[24] T. Rabczuk, G. Zi, S. Bordas, and H. Nguyen Xuan, "A geometrically nonlinear three dimensional cohesive crack method for reinforced concrete structures", *Eng. Frac. Mech.*, vol. 75, pp. 4740–4758, 2008. doi:10.1016/j.engfracmech.2008.06.019.

[25] R. Seifi and K. Y. Nafiseh, "Experimental and numerical studies on buckling of cracked thin plates under full and partial compression edge loading", *Thin. Wall. Struct.*, vol. 19, pp. 1504–1516, 2011. doi:10.1016/j.tws.2011.07.010.

[26] D. Schillinger, M. J. Borden, and H. Stolarski, "Isogeometric collocation for phase-field fracture models", *Comp. Meth. Appl. Mech. Eng.*, vol. 284, pp. 583–610, 2015. doi:10.1016/j.cma.2014.09.032.

[27] J. H. Song and T. Belytschko, "Dynamic fracture of shells subjected to impulsive loads", *J. Appl. Mech. Trans. Asm.*, vol. 76, pp. 051–301, 2009.

[28] H. Ulmer, M. Hofacker, and C. Miehe, "Phase field modeling of fracture in plates and shells", *Proc. App. Math. Mech.*, vol. 12, pp. 171–172, 2012. doi:10.1002/pamm.201210076.

[29] G. N. Wells and L. J. Sluys, "A new method for modelling cohesive cracks using finite elements", *Int. J. Num. Meth. Eng.*, vol. 50, pp. 2667–2682, 2001. doi:10.1002/nme.143.

[30] K. G. Wang, P. Lea, and C. Farhat, "A computational framework for the simulation of high-speed multi-material fluid–structure interaction problems with dynamic fracture", *Int. J. Num. Meth. Eng.*, vol. 104, pp. 585–623, 2015. doi:10.1002/nme.4873.

[31] H. D. Duc, B. Q. Tinh, N. D. Duc, and F. Fazuyoshi, "Hybrid phase field simulation of dynamic crack propagation in functionally graded glass-filled epoxy", *Compos. Part B: Eng.*, vol. 99, pp. 266–276, 2016. doi:10.1016/j.compositesb.2016.06.016.

[32] G. Bhardwaj, I. V. Singh, B. K. Mishra, and V. Kumar, "Numerical simulations of cracked plate using XIGA under different loads and boundary conditions", *Mech. Adv. Mater. Struct.*, vol. 23, no. 6, pp. 704–714, 2016. doi:10.1080/15376494.2015.1029159.

[33] J. H. Kim and H. P. Glaucio, "On fracture criteria for mixed-mode crack propagation in functionally graded materials", *Mech. Adv. Mater. Struct.*, vol. 14, pp. 227–244, 2007. doi:10.1080/15376490600790221.

[34] R. Kolahchi and A. M. M. Bidgoli, "Size-dependent sinusoidal beam model for dynamic instability of single-walled carbon nanotubes", *Appl. Math. Mech. -Engl. Ed.*, vol. 37, no. 2, pp. 265–274, 2016. doi:10.1007/s10483-016-2030-8.

[35] R. Kolahchi, H. Hosseini, and M. Esmailpour, "Differential cubature and quadrature-Bolotin methods for dynamic stability of embedded piezoelectric nanoplates based on visco-nonlocal-piezoelasticity theories", *Compos. Struct.*, vol. 157, pp. 174–186, 2016. doi:10.1016/j.compstruct.2016.08.032.

[36] M. Zamanian, R. Kolahchi, and M. R. Bidgoli, "Agglomeration effects on the buckling behaviour of embedded concrete columns reinforced with SiO2 nano-particles", *Wind Struct.*, vol. 24, no. 1, pp. 43–57, 2017. doi:10.12989/was.2017.24.1.043.

[37] A. J. Arani and R. Kolahchi, "Buckling analysis of embedded concrete columns armed with carbon nanotubes", *Comput. Concr.*, vol. 17, no. 5, pp. 567–578, 2016. doi:10.12989/cac.2016.17.5.567.

[38] R. Kolahchi, M. Safari, and M. Esmailpour, "Dynamic stability analysis of temperature-dependent functionally graded CNT-reinforced visco-plates resting on orthotropic elastomeric medium", *Compos. Struct.*, vol. 150, pp. 255–265, 2016. doi:10.1016/j.compstruct.2016.05.023.

[39] R. Kolahchi and A. Cheraghbak, "Agglomeration effects on the dynamic buckling of viscoelastic microplates reinforced with SWCNTs using Bolotin method", *Nonlinear Dyn.*, vol. 90, pp. 479–492, 2017. doi:10.1007/s11071-017-3676-x.

[40] R. Kolahchi, M. S. Zarei, M. H. Hajmohammad, and A. N. Oskouei, "Visco-nonlocal-refined Zigzag theories for dynamic buckling of laminated nanoplates using differential cubature-Bolotin methods", *Thin-Walled Struct.*, vol. 113, pp. 162–169, 2017. doi:10.1016/j.tws.2017.01.016.

[41] B. S. Bilouei, R. Koulahchi, and M. R. Bidgoli, "Buckling of concrete columns retrofitted with Nano-Fiber Reinforced Polymer (NFRP)", *Comput. Concr.*, vol. 18, no. 5, pp. 1053–1063, 2016. doi:10.12989/cac.2016.18.5.1053.

[42] H. Madani, H. Hosseini, and M. Shokravi, "Differential cubature method for vibration analysis of embedded FG-CNT-reinforced piezoelectric cylindrical shells subjected to uniform and non-uniform temperature distributions", *Steel Compos. Struct.*, vol. 22, no. 4, pp. 889–913, 2016. doi:10.12989/scs.2016.22.4.889.

[43] M. S. Zarei, R. Kolahchi, M. H. Hajmohammad, and M. Maleki, "Seismic response of underwater fluid-conveying concrete pipes reinforced with SiO2 nanoparticles and fiber reinforced polymer (FRP) layer", *Soil Dyn. Earthquake Eng.*, vol. 103, pp. 76–85, 2017. doi:10.1016/j.soildyn.2017.09.009.